Designing a self-healing protective film on a lithium metal anode for long-cycle-life lithium-oxygen batteries

Yue Yu[a,b], Yan-Bin Yin[e], Jin-Ling Ma[a,c], Zhi-Wen Chang[a,c], Tao Sun[a,c], Yun-Hai Zhu[a,d], Xiao-Yang Yang[a,d], Tong Liu[a,b], Xin-Bo Zhang[a,b,*]

[a] State Key Laboratory of Rare Earth Resource Utilization, Changchun Institute of Applied Chemistry, Chinese Academy of Sciences, Changchun 130022, PR China
[b] University of Science and Technology of China, Hefei 230026, Anhui, PR China
[c] University of Chinese Academy of Sciences, Beijing 100049, PR China
[d] Key Laboratory of Automobile Materials (Jilin University), Ministry of Education, Department of Materials Science and Engineering, Jilin University, Changchun 130022, PR China
[e] Dalian Institute of Chemical Physics, Chinese Academy of Sciences, 457 Zhongshan Road, Dalian 116023, PR China

ARTICLE INFO

ABSTRACT

The development of high energy density Li-O$_2$ batteries is hindered by many scientific and technological challenges, especially the intrinsic corrosion of the lithium metal anode induced by O$_2$, H$_2$O and discharge intermediates in electrolytes. In response, as a proof-of-concept experiment, we first propose and demonstrate a facile and highly efficient strategy for the *in situ* growth of a self-healing protective film on a lithium metal anode, wherein tetraethyl orthosilicate plays a key role as a novel film-forming electrolyte additive. This additive can spontaneously and effectively react with the main component of the detrimental surface corrosion layer (lithium hydroxide) on the lithium metal anode, forming a self-healing protective film with dynamic repair ability during the cycling process. Unexpectedly, the protected lithium metal anode endows the Li-O$_2$ batteries with significantly improved battery cycle performance (up to 144 cycles). We consider that our facile, low-cost, and highly effective lithium protection strategy presents a new avenue to address the daunting corrosion problem of lithium metal anodes in Li-O$_2$ batteries, which can be easily extended to other metal-O$_2$ battery systems such as Na-O$_2$ batteries.

1. Introduction

Next-generation batteries with high energy density are urgently needed for the development of electric vehicles and smart grid storage [1]. The lithium-oxygen (Li-O$_2$) battery is a promising candidate because of its extremely high specific energy density (3500 Wh kg^{-1}), which is approximately tenfold higher than that of lithium-ion batteries [2–5]. A typical Li-O$_2$ battery is composed of an oxygen cathode and a lithium metal anode. The use of a reversible lithium metal anode is crucial to obtain high energy density in the Li-O$_2$ battery owing to its low density (0.53 g cm^{-3}), ultrahigh specific energy density (3860 mA h g^{-1}) and extremely low negative electrochemical potential (-3.04 V vs the standard hydrogen electrode) [6,7]. However, the intrinsic corrosion induced by O$_2$, H$_2$O and discharge intermediates (especially the superoxide radical anion O$_2^-$ and the peroxide radical anion O$_2^{2-}$) in the electrolyte leads to inferior reversibility of lithium metal anodes in Li-O$_2$ batteries [8–10]. Worse, lithium metal anodes

face the danger of being depleted, which can lead to total battery failure [11–13]. Therefore, it is important to develop a facile but effective strategy to protect Li metal anodes in Li-O$_2$ batteries.

Recently, several creative protection methods for lithium metal anodes in Li-ion batteries have been reported. However, most of these strategies are not very effective for the protection of Li metal anodes in Li-O$_2$ batteries. For example, a number of studies have demonstrated that the use of a 3D structure with a high specific surface area can alleviate large volume changes and prevent uncontrollable dendrite growth [14–17]. Unfortunately, owing to the presence of O$_2$, H$_2$O and strong oxidative discharge intermediates in the electrolyte of Li-O$_2$ batteries, a high specific surface area of the 3D structured electrode would expedite the depletion of the deposited Li and battery failure. Therefore, the protection of Li metal anodes in Li-O$_2$ batteries is more challenging than that in Li-ion or Li-S batteries. To date, lithium protection approaches in Li-O$_2$ batteries are relatively unexplored and remain limited to tailored polymer separators [18–20] and protection

films [21,22]. Unfortunately, these methods are still plagued by various drawbacks, such as multistep and time/cost-consuming preparation processes and, in particular, the unsatisfactory stability of polymer materials and protection films in a highly corrosive and O_2^-/O_2^{2-}-containing environment [23]. Therefore, it is urgently desired but also a great challenge to develop a facile, low-cost, effective and long-lasting protection strategy to protect lithium metal anodes in Li-O$_2$ batteries.

Silane pretreatment of Li metal anodes has been reported to produce a protection film for a stable stripping/plating process in Li-ion battery on account of reacting with hydroxyl groups on lithium metal to generate a protection film [24,25]. However, the low concentration of hydroxyls on fresh metal lithium which makes the film too sparse and the pretreated method itself cannot provide an efficacious and long-acting protection. Herein, as a proof-of-concept experiment, we propose and demonstrate a facile, low-cost, and very effective strategy to protect the lithium metal anode in Li-O$_2$ batteries *in situ* by using tetraethyl orthosilicate (TEOS) as a novel film-forming electrolyte additive. This additive spontaneously reacts with the main lithium corrosion product, lithium hydroxide (LiOH), to form a Si-O-containing film on the lithium metal anode in real time and provide a dynamic self-healing effect. This film could effectively prevent lithium from further corrosion by O$_2$, H$_2$O, and discharge intermediates in the electrolyte, thus effectively improving the stability of the lithium anode. Unexpectedly, the protected lithium metal anode endows the Li-O$_2$ batteries with significantly improved battery cycle performance (up to 144 cycles).

2. Materials and methods

2.1. Chemicals and materials

TEGDME, LiCF$_3$SO$_3$, TEOS, RuCl$_3$·xH$_2$O, KO$_2$ and NMP were purchased from Aladdin Reagent. Pluronic F127 was purchased from Sigma-aldrich. Carbon paper was purchased from Torray Japan. Lithium sheets were purchased from China Energy Lithium Co., Ltd. Polyvinylidene fluoride (PVDF) was purchased from Arkema. CNTs were purchased from Cnano Technology Ltd. Super P carbon was purchased from the TIMCAL Graphite & Carbon.

2.2. TPL anode preparation

TPL was prepared by placing untreated lithium into TEOS for 5 min and then dried in an Ar-filled glove box at room temperature.

2.3. FTIR sample preparation

In a glove box, 0.355 g KO$_2$ was added to 5 ml of different types of electrolyte (common electrolyte, TEOS additive electrolyte or pure TEOS) and stirred for 100 h. Then, all the samples were dropped onto a transparent KBr pellet for testing.

2.4. Li-O$_2$ battery preparation and measurements

The electrolyte solution was prepared by dissolving 1 M LiCF$_3$SO$_3$ in TEGDME with or without 5 wt% TEOS electrolyte additive in an Ar-filled glove box (< 0.1 ppm O$_2$ and H$_2$O). Super P and PVDF binder in a weight ratio of 4:1 were uniformly dissolved in NMP and subsequently sprayed onto carbon paper (TGP-H-060, Toray, φ = 12 mm) as the air cathode. Then, it was dried at 80 °C for 1 d under vacuum to remove residual solvent. The Ru/CNTs were also prepared using our previously reported method for long time galvanostatic cycling tests with a specific capacity of 1000 mA h g^{-1} [26]. Briefly, 200 mg CNTs, 1 g Pluronic F127 and 200 mg RuCl$_3$·xH$_2$O were dispersed in distilled water and then stirred well. The obtained mixture was dried and then heated at 300 °C for 3 h under 5% H$_2$/Ar in tubular furnace. The final loading mass of

cathode was approximately 0.45 mg cm^{-2}. Next, 2025 coin cells with holes were assembled using a lithium sheet as the anode. Then, the GF separator was placed on the Li anode, and 80 μl of electrolyte was injected, followed by the addition of the cathode and Ni foam. Finally, the coin cells were pressurized using an automatic crimping machine. The batteries were prepared in an Ar-filled glove box (< 0.1 ppm O$_2$ and H$_2$O).

2.5. Characterization

Powder X-ray diffraction (XRD) measurement was performed using a Bruker D8 Focus Powder X-ray diffractometer with Cu Kα (λ = 0.15405 nm) radiation (40 kV, 40 mA). Scanning electron microscopy (SEM) and element mapping were carried out with a field emission scanning electron microanalyzer (Hitachi S4800) operated at an accelerating voltage of 10 kV. X-ray photoelectron spectroscopy (XPS) analysis was carried out on a VG Scientific ESCALAB MKII X-ray photoelectron spectrometer using an Al Kα source. FTIR tests were carried out on a Nicolet iS5 spectrometer. The galvanostatic charge/discharge tests were conducted with a Land CT2001A at room temperature in an O$_2$ chamber. Electrochemical impedance spectroscopy (EIS) and cyclic voltammetry (CV) tests were performed using a BioLogic VMP3 electrochemical workstation.

3. Results and discussion

Fig. 1 demonstrates the hypothetical protective film formation process in Li-O$_2$ batteries with TEOS electrolyte additive. Generally, when the lithium metal anode operated in Li-O$_2$ batteries, the highly corrosive environment will turn the surface of lithium metal anode to the detrimental corrosion products LiOH. But in the Li-O$_2$ batteries with the TEOS additive, the corrosive product LiOH is a necessary ingredient for the *in situ* film formation process, which will react with TEOS electrolyte additive via a non-hydrolytic sol-gel process just like the reactions in Fig. S1. LiOH can react with TEOS, then forming a thin layer of lithium silicate (reaction 1 and reaction 2). If this reaction is continued, the SiO$_2$ will be formed through the reaction (reaction 3) in the end.

For the sake of verifying the above hypothesis, X-ray photoelectron spectroscopy (XPS) was employed to analyze the elemental composition of the protective film on lithium metal anode in Li-O$_2$ batteries with TEOS electrolyte additive after one cycle. As shown in Fig. 2a, the XPS spectra of Li 1s can be deconvoluted into two peaks at 54.9 and 55.4 eV. The former peak can be assigned to Li-O which derive from the thin film of Li$_x$SiO$_y$ formed on Li metal anodes, whereas the latter can be ascribed to a small quantity of Li$_2$CO$_3$ formed on Li metal anodes during cycling [9]. The Si 2p spectrum in Fig. 2b can be fitted by four peaks. The peaks centered at 101.1 and 101.9 eV can be assigned to Li$_x$SiO$_y$ and the other two peaks belong to SiO$_2$. In the C 1s spectrum shown in Fig. 2c, the various peaks located at 284.5, 285.1, 287.1 and 290 eV could be assigned to functional groups related to C-C, C-H, C-O and carbonate groups. For the O 1s spectrum in Fig. 2d, the peaks at 530.2, 531.2, 531.7 and 532.7 eV correspond to Li$_x$SiO$_y$, Li$_2$CO$_3$, SiO$_2$ and C-O functional groups. From the above, the presence of Li$_x$SiO$_y$ and SiO$_2$ in the protective film which results from the reactions in Fig. S1 could be determined.

To further demonstrate the effect of TEOS electrolyte addition, the electrochemical performance of Li-O$_2$ batteries with BL, TPL and TAL were evaluated. First, the cyclic voltammetry (CV) curves under O$_2$ and Ar atmospheres were examined (Fig. S2a,b). The batteries under Ar showed negligible current densities (Fig. S2a), whereas the same battery in O$_2$ exhibited obvious cathodic and anodic peaks at potentials consistent with those in the literatures (Fig. S2b), verifying that the TEOS electrolyte additive does not affect the main reaction of the Li-O$_2$ battery [27,28]. Fig. 3 shows the discharge-charge curves and terminal-potential profiles of three different types of lithium metal anodes in Li-
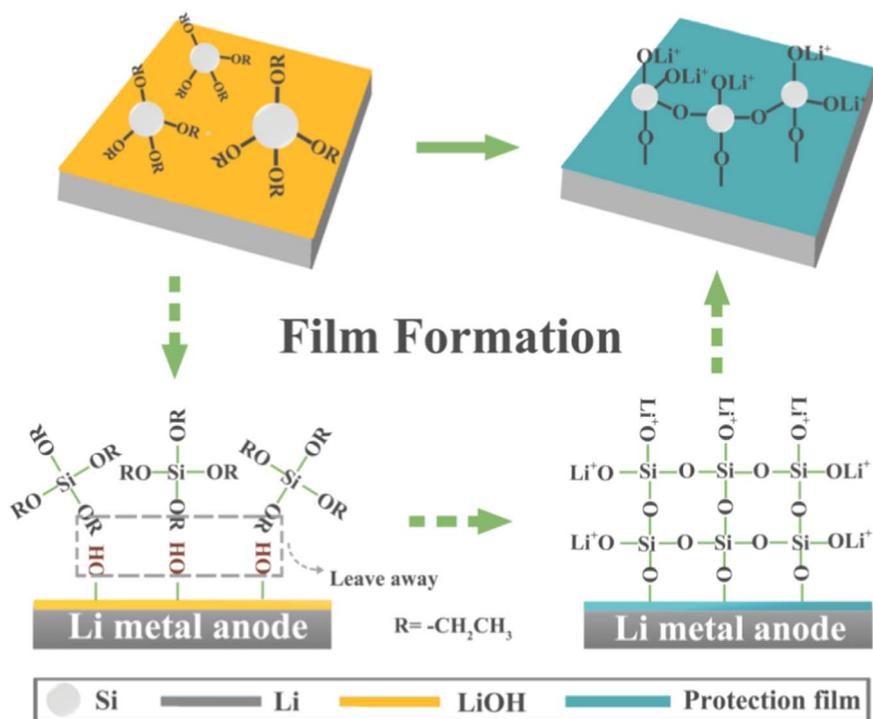
Fig. 1. Schematic illustration of the lithium protection film formation mechanism on TAL in Li-O_2 batteries.

O_2 batteries. It was explicitly found that the Li-O_2 batteries with BL and TPL only cycled for 70 cycles and 88 cycles, respectively, when the cut-off voltage was restricted to 2.0 V. Encouragingly, 144 discharge-charge cycles were obtained with TAL under the same conditions. The significant amelioration of cycle performance is attributed to the more stable lithium surface and effectively reduced corrosion [18,21,29]. The rate performance was displayed in Fig. S8, the Li-O_2 batteries with TEOS

electrolyte additive behave a better rate performance even at the high current density of 1000 mA g^{-1}. Though the rate performance of cathode should be similar in three kinds of batteries, the rate performance of anodes have been improved a lot after protection in Fig. S9. The symmetrical batteries with TEOS addition exhibit much more stable rate voltage profiles than those without protection even at a high current density of 0.5 mA cm^{-2} which amount to the current density of 1729 mA
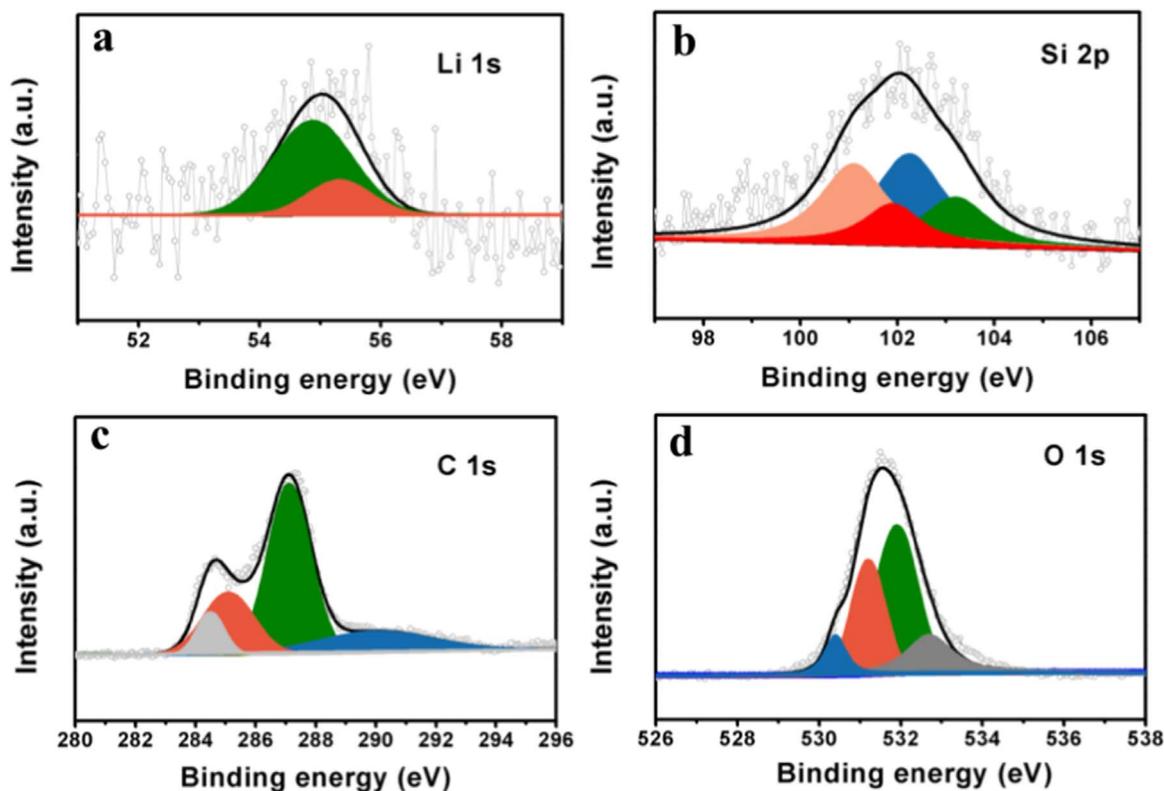
Fig. 2. The (a) Li 1s, (b) Si 2p, (c) C 1s and (d) O 1s XPS spectra of the TAL anode in Li-O_2 battery after one cycle.
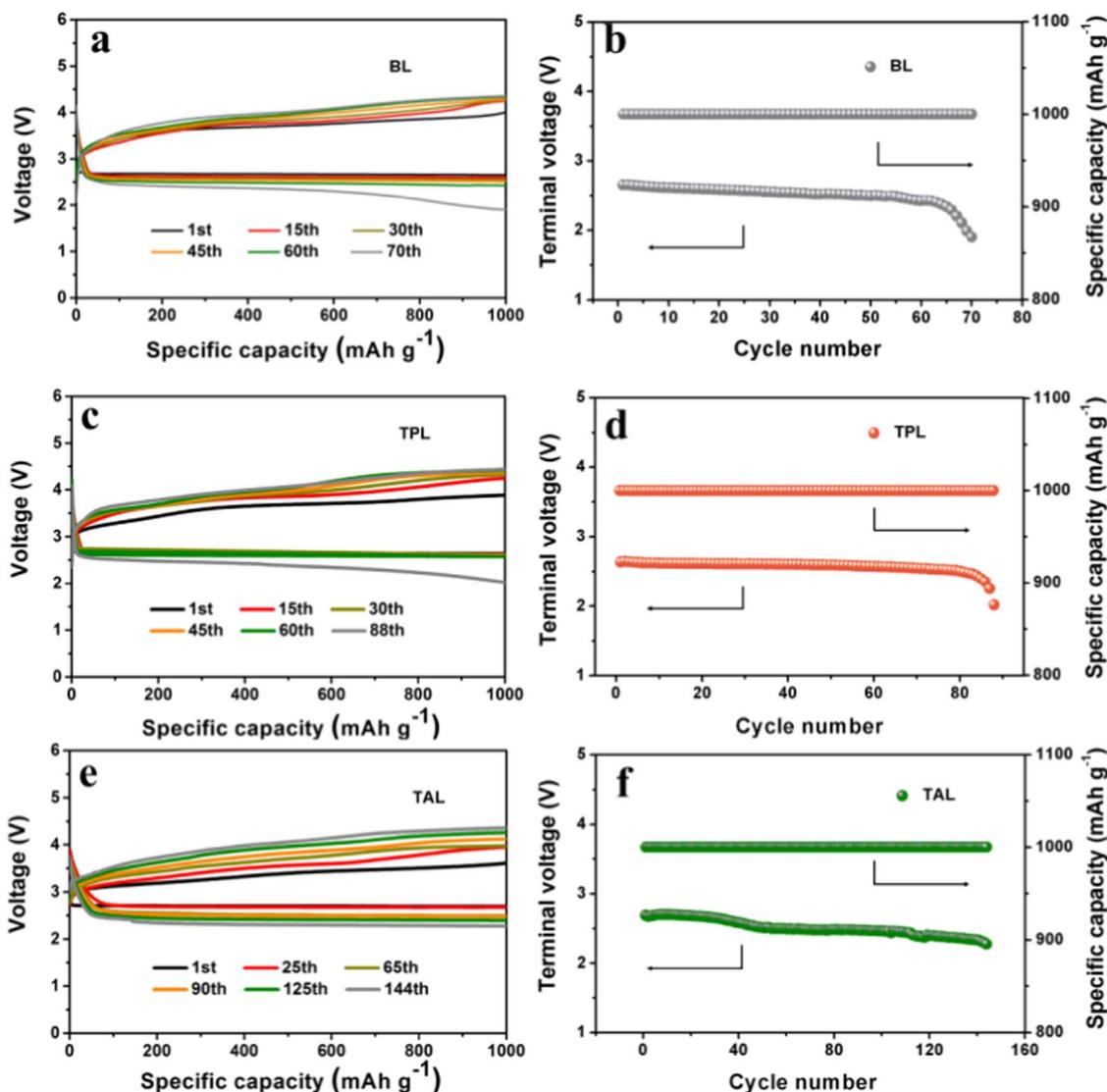
Fig. 3. Discharge-charge curves of Li-O$_2$ batteries with a) BL, c) TPL, and e) TAL anode and the corresponding terminal voltage curves with b) BL, d) TPL, f) TAL. All battery performances shown in this figure were tested with a fixed capacity of 1000 mA h g^{-1} at a current density of 300 mA g^{-1}.

g^{-1} in Li-O$_2$ batteries. This improvement can be attributed to the fact that the TEOS addition can help to form a stable protection film on lithium and build a stable Li/electrode interface [30]. To further demonstrate whether the TEOS electrolyte additive influences the discharge process of the Li-O$_2$ battery, full discharge curves and the XRD curves, SEM images of discharge products were examined. Fig. S10 shows the discharge curves of Li-O$_2$ batteries with three different types of lithium metal anodes. It can be seen that they all exhibit similar discharge capacities, which indicates that the TEOS electrolyte additive does not affect the discharge process of the Li-O$_2$ batteries. In Fig. S14, the XRD patterns and SEM images show that the discharge products of Li-O$_2$ batteries with three different types of metal anodes are crystalline toroid-shaped Li$_2$O$_2$ particles, similar to the discharge products of Li-O$_2$ batteries in other literature reports [31–33].

The electrochemical stability of Li-O$_2$ batteries with TEOS electrolyte additive is also examined. In Fig. S15, compared with the poor electrolyte stability of Li-O$_2$ batteries without TEOS electrolyte additive, the linear sweep voltammetry (LSV) curves of Li-O$_2$ batteries with TEOS electrolyte additive display an electrolyte window of around 4.25 V vs Li/Li$^+$ which is 0.45 V higher than the batteries without TEOS additive. To ascertain the reason of this improvement, we tested the electrochemical stable window of pure TEGDME, pure TEOS and the TEOS with saturated Li salt (the solubility of LiCF$_3$SO$_3$ in TEOS is

much lower than 1 M). As Fig. S16 shows, the electrochemical stability window of pure TEGDME is much lower than pure TEOS and TEOS with saturated Li salt, which can indicate the good electrochemical stability of TEOS. We conjecture that the stable TEOS addition has a positive interaction with the unstable TEGDME and stabilize the electrolyte itself. In addition, because the solution of LiCF$_3$SO$_3$ in TEOS is very little, so the TEOS itself may be act as an "inert" diluent, which form a localized high concentration electrolyte and behave a wider electrochemical stability window [34]. Besides, to confirm the chemical stability of TEOS in the strongly oxidative environment of Li-O$_2$ batteries, KO$_2$ was added to the electrolyte and stirred for 100 h for Fourier transform infrared spectroscopy (FTIR) tests [35,36]. As shown in Fig. S17, although the peaks at 1128 cm^{-1} and 1300 cm^{-1} become the peak at 1272 cm^{-1} after adding KO$_2$, the same phenomenon can also be observed upon comparing the spectra of the common electrolyte without and with KO$_2$ after stirred for 100 h. This result can be attributed to the instability of common electrolyte, which is a general and thorny problem in Li-O$_2$ batteries [37,38]. To further demonstrate the stability of TEOS, the FTIR spectra of pure TEOS without and with KO$_2$ after stirred for 100 h were analyzed and are shown in Fig. S18. There is also no obvious difference between them, indicating the relative stability of TEOS in the strongly oxidative environment in Li-O$_2$ batteries.

The electrochemical impedance spectrum (EIS) is a general and effective tool to illustrate the corrosion condition of lithium metal anodes because the by-products resulting from side reactions on anodes can increase the resistance of the battery [21]. The EIS results of storing for different time with three different types of anodes are shown in Fig. S19. With the storage time prolonging, the corresponding impedance values of batteries with BL and TPL increase sharply, indicating the more severe corrosion from the electrolyte and O_2. In sharp contrast, far fewer impedance changes are observed even after 96 h in a Li-O_2 battery with TAL, which can be attributed to the effective and long-lasting self-healing film on the lithium metal anode. The EIS results of Li-O_2 batteries with different anodes after different cycles are also provided in Fig. S20. As the cycling process goes on, the impedance values of TAL grows much lower than those of BL and TPL. In order to better demonstrate the corrosion condition of lithium metal anode, we disassemble the Li-O_2 battery with BL, TPL and TAL after 50 cycles and reassemble the Li/Li symmetrical batteries. The symmetrical batteries exclude the disturbance of electrolyte and cathode and focus on the corrosion condition of lithium. The increase of the impedance is wholly resulted from the corrosion of lithium and can better reveal the corrosion effect of lithium metal anode. In Fig. S21, the impedance of symmetrical batteries with TAL is much lower than those with BL and TPL which indicate the good protection effect of TEOS electrolyte addition. All these improvements further verify the effect of the TEOS electrolyte additive, which can provide effective and long-lasting protection to stabilize the interface of lithium metal anodes.

To clearly reveal the corrosion condition of the lithium surface before and after protection, the composition and morphological evolution of three different types of lithium metal anodes were investigated by field emission scanning electron microscopy (FESEM) and X-ray diffraction (XRD). The amount of LiOH can be regarded as the corrosion degree of the lithium metal anode in the Li-O_2 battery [21]. As shown in Fig. 4a, the XRD pattern of BL shows an obvious LiOH peak after 10 cycles, indicating that the Li suffers a strong degree of corrosion. As the cycling processes, the XRD pattern of BL after 50 cycles shows much stronger LiOH peaks, indicating that a large amount

of LiOH accumulated on the Li metal surface in the absence of protection. As shown in Fig. 4e, the XRD diffraction peaks of TPL indicate less corrosion compared with that of BL. However, in the subsequent cycles, obvious LiOH peaks signify the limited protective effect during cycles without dynamic repair and finally result in the failure to protect Li metal anodes. In sharp contrast, the XRD peaks of TAL display no obvious LiOH signal until 50 cycles, confirming that the TEOS electrolyte additive can provide long-lasting protection (Fig. 4i). The relative morphological evolution of the three types of lithium metal anodes was obtained from SEM images. The surface morphology of TAL after one cycle displayed a uniform and smooth surface morphology (Fig. 4j), which is a result of the reaction between TEOS and LiOH that generates the protective film. As the cycling goes on, the protection results show striking differences among the three types of lithium metal anodes. The surface morphology of BL after cycles is much rougher compared with that of TPL and TAL, indicating the serious corrosion of the Li anode without any protection (Fig. 4b, c, d). The TPL shows an alleviated corrosion condition compared with that of BL (Fig. 4f, g, h), but its surface is more rugged than that of TAL. As shown in Fig. 4j, k, l, the morphological evolution of TAL shows no obvious rough surfaces and relatively uniform morphology even after 50 cycles, confirming that the TEOS electrolyte additive can provide effective and long-lasting protection for lithium metal anodes. Furthermore, the exhaustive stripping tests of three kinds of lithium after 50 cycles were carried out to verify the protection effect in Fig. S22. Compared with the exhaustive stripping capacity of pristine Li sheet (44.748 mA h), the remaining capacity of TAL after 50 cycles is 40.188 mA h while that of TPL and BL is only 29.474 mA h and 16.282 mA h which can verify the excellent long-lasting protection of TEOS. All these results can confirm the effectiveness of TEOS addition on lithium protection in Li-O_2 batteries.

This long-lasting and excellent protection of TEOS electrolyte addition can be attributed to the self-healing effect due to the reaction between TEOS and LiOH. For purpose of illustrating this particular effect during the cycling process, TPL was chosen as the contrast material. First, Si element mapping measurement was used to display
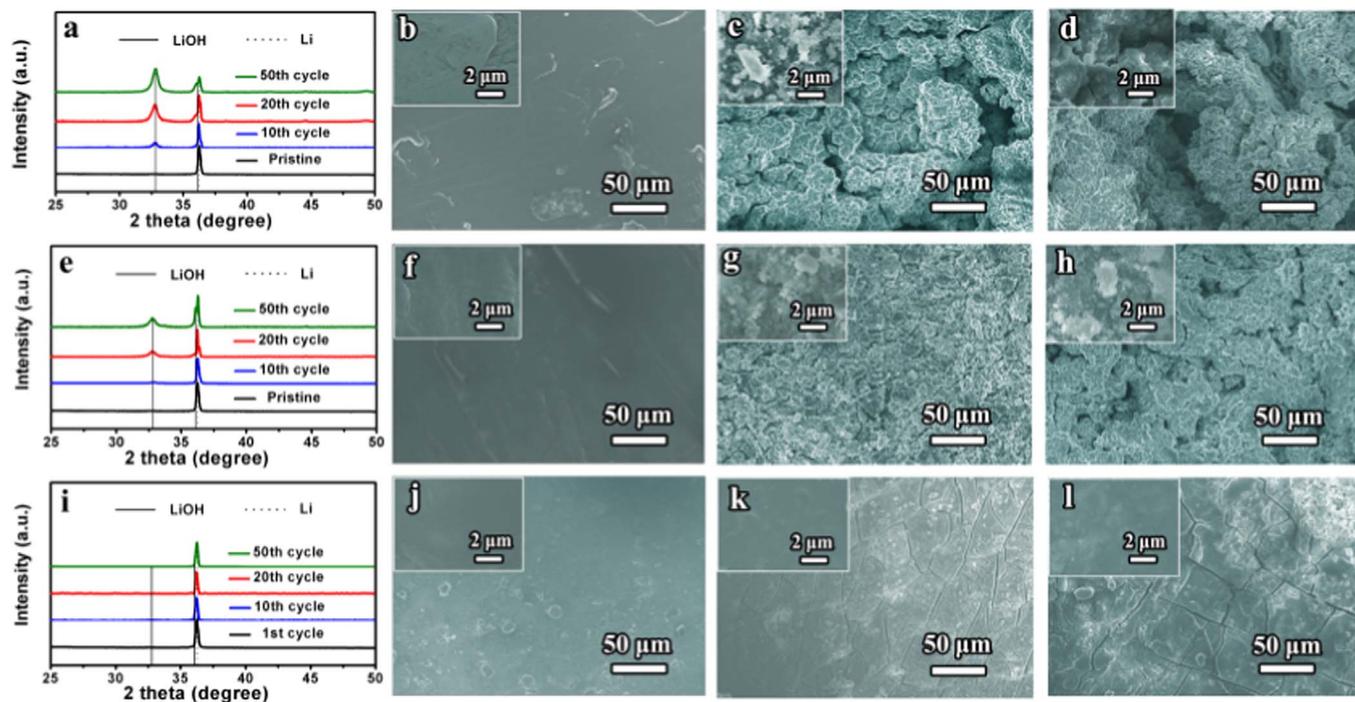
Fig. 4. XRD patterns taken from a) BL, e) TPL, and i) TAL anodes at different cycles. SEM images of BL anode morphological evolution b) before cycling, c) after the 20th cycle, and d) after the 50th cycle. SEM images of TPL anode morphological evolution f) before cycling, g) after the 20th cycle, and h) after the 50th cycle. SEM images of TAL anode morphological evolution j) after the 1st cycle, k) after the 20th cycle, and l) after the 50th cycle. The insets of SEM images are high-magnification versions of the corresponding SEM images of the Li metal anode at different cycles.
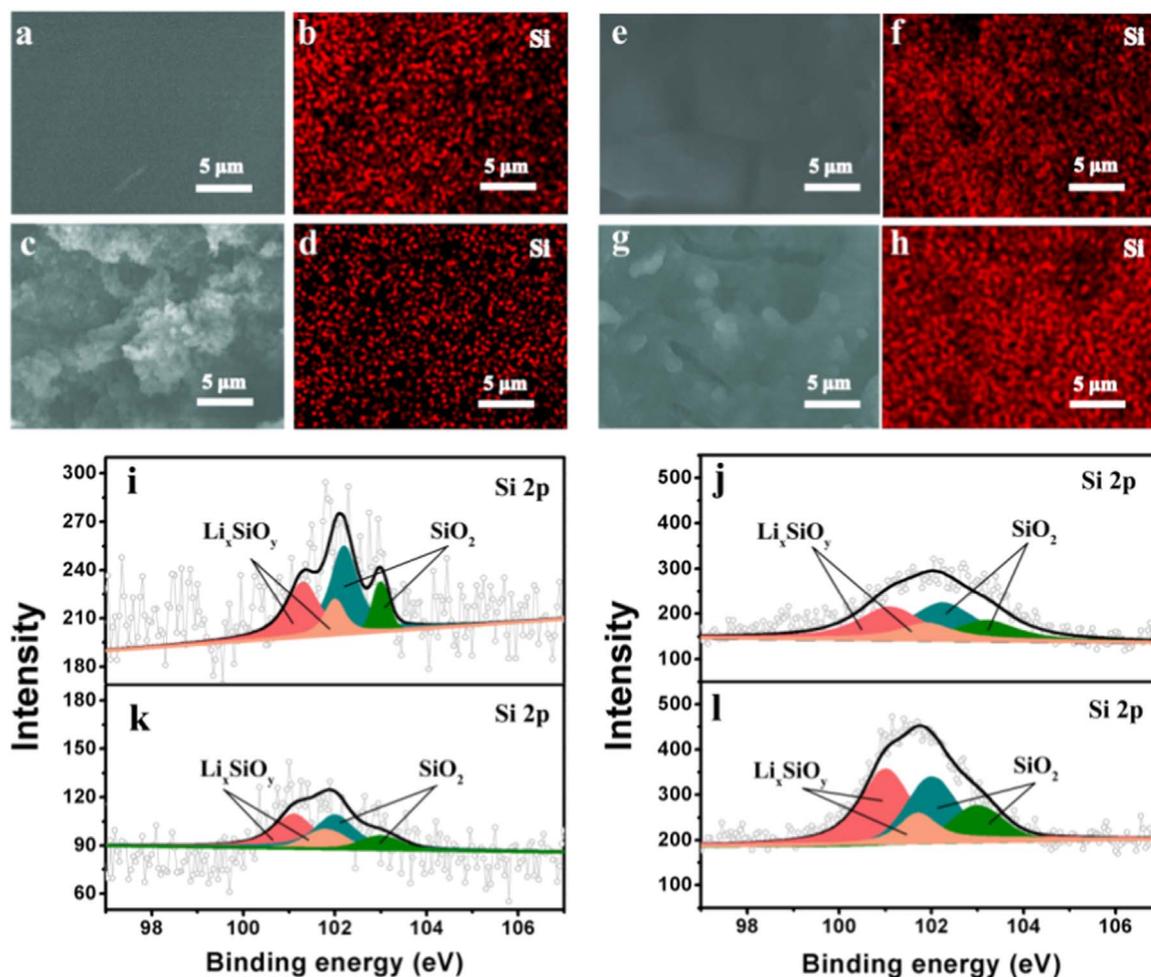
Fig. 5. a) SEM images of TPL and b) corresponding Si element mapping of TPL before cycling, c) SEM images of TPL and d) corresponding Si element mapping of TPL after 50 cycles. e) SEM images of TAL and f) corresponding Si element mapping of TAL after one cycle, g) SEM images of TAL and h) corresponding Si element mapping of TAL after 50 cycles. Si 2p XPS spectra of TPL i) before cycling, k) after 50 cycles. Si 2p XPS spectra of TAL j) after one cycle, l) after 50 cycles.

the changes in surface element distribution on two kinds of lithium metal anodes. In Fig. 5a-d, less Si element is present on the TPL surface after 50 cycles than before, indicating that the Si-O coating layer is damaged and not repaired, thus leading to protection failure. In sharp contrast, Fig. 5e-h shows a strong Si element signal before and after the cycles, verifying that the self-healing effect of protection film can effectively improve the problem of the film being damaged without repair during cycling. Then the Si 2p XPS spectra of the two kinds of metal anodes in Li-O$_2$ batteries before and after 50 cycles were used to further confirm the self-healing effect of the film during the cycling process. In Fig. 5i and k, although the TPL surface composition

contains Si-O before and after 50 cycles, the much weaker peaks indicate a reduced amount of Si-O due to the damage to the protection film during cycles. In sharp contrast, as shown in Fig. 5j and l, Si-O is still the main surface component of TAL in Li-O$_2$ batteries after 50 cycles with no decrease in content, which demonstrates that the surface composition scarcely changed after 50 cycles owing to the long-lasting self-healing protective effect of the TEOS electrolyte additive.

According to the above results, a more preferable protection of TAL than TPL and BL can be illustrated as follows. As Fig. 6 shows, without any effective protective measures, BL will be corroded to LiOH rapidly in the highly corrosive environment of the Li-O$_2$ battery. The film
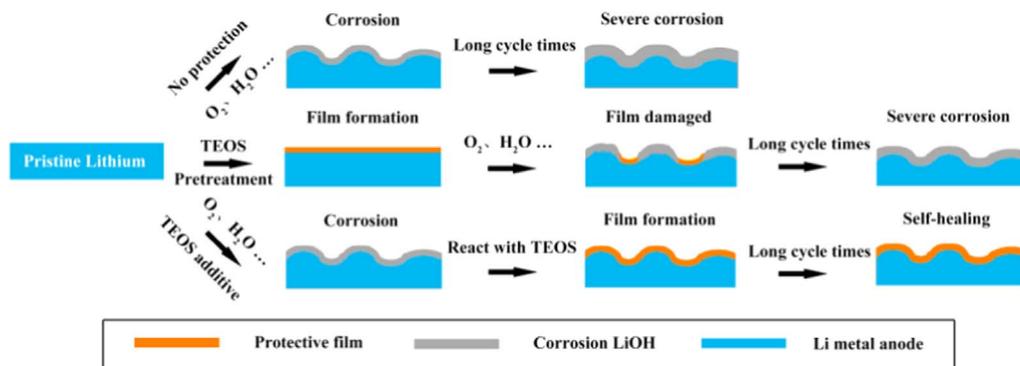
Fig. 6. The protection mechanism comparison of the three kinds of lithium metal anodes.

formed on TPL stabilizes the lithium metal anode to some extent due to the reaction between the hydroxyl on Li and the TEOS. However, the protective film will be damaged during long-term cycling in the highly corrosive environment and finally lead to protection failure. In fact, the failure of the protective film is still a daunting challenge for any protection layer without dynamic repair ability. In sharp contrast, with the help of the TEOS electrolyte additive, after corrosion LiOH forms on the Li metal surface, TEOS will react with LiOH to form an *in situ* protective film. Even when the film is damaged due to long-term cycling in the highly corrosive environment, the TEOS in the electrolyte will provide a self-healing effect by reacting with bare LiOH to dynamically repair the film, thus improving the electrochemical performance and the reversibility of lithium metal anodes.

4. Conclusion

In summary, this study is the first to propose and demonstrate a facile, low-cost, very effective strategy to protect the lithium metal anode *in situ* by using TEOS as a novel electrolyte additive in $Li-O_2$ batteries, which can react with the intrinsic anodic corrosion LiOH to form a protective film and provide a dynamic self-healing repair effect. With this protection method, there is no evident LiOH peak in the XRD patterns after 50 cycles, and the morphology remains much smoother than in the control batteries. Most importantly, the additive also benefits the battery cycle performance (up to 144 cycles) of $Li-O_2$ batteries. All these results are considered to stem from the *in situ* growth of a self-healing protective film, which provides a dynamic repair effect for lithium metal anodes in $Li-O_2$ batteries. Based on these results, this effective, long-lasting, facile and low-cost protection strategy will encourage further studies on the protection of Li metal anodes in $Li-O_2$ batteries, even in $Na-O_2$ batteries.

Acknowledgments

Notes

The authors declare no competing financial interest.

Appendix A. Supporting information

Supplementary data associated with this article can be found in the online version at doi:10.1016/j.ensm.2019.01.009.

References

[1] J.-M. Tarascon, M. Armand, Building better batteries, Nature 452 (2008) 652–657.
[2] P.G. Bruce, S.A. Freunberger, L.J. Hardwick, J.M. Tarascon, Li-O₂ and Li-S batteries with high energy storage, Nat. Mater. 11 (2011) 19–29.
[3] M. Haro, N. Vicente, G. Garcia-Belmonte, Oxygen reduction reaction promotes Li⁺ desorption from cathode surface in Li-O₂ batteries, Adv. Mater. Interfaces 2 (2015) 1500369.
[4] C.T.-C.W. Snehashis Choudhury, Wajdi I. Al Sadat, Zhengyuan Tu, Sampson Lau, Michael J. Zachman, Lena F. Kourkoutis, Lynden A. Archer, Designer interphases for the lithium-oxygen electrochemical cell, Sci. Adv. 3 (2017) e1602809.
[5] C.P. Grey, J.M. Tarascon, Sustainability and in situ monitoring in battery development, Nat. Mater. 16 (2016) 45–56.
[6] X. Liang, Q. Pang, I.R. Kochetkov, M.S. Sempere, H. Huang, X. Sun, L.F. Nazar, A facile surface chemistry route to a stabilized lithium metal anode, Nat. Energy 2 (2017) 17119.
[7] C.-F.L. Alexander, C. Kozen, Alexander J. Pearse, Marshall A. Schroeder, Xiaogang Han, Liangbing Hu, Sang-Bok Lee, Gary W. Rubloff, Malachi Noked, Next-generation lithium metal anode engineering via atomic layer deposition, ACS Nano 9 (2015) 5884–5892.
[8] H. Lee, D.J. Lee, J.-N. Lee, J. Song, Y. Lee, M.-H. Ryou, J.-K. Park, Y.M. Lee, Chemical aspect of oxygen dissolved in a dimethyl sulfoxide-based electrolyte on lithium metal, Electrochim. Acta 123 (2014) 419–425.
[9] R.S. Assary, J. Lu, P. Du, X. Luo, X. Zhang, Y. Ren, L.A. Curtiss, K. Amine, The effect of oxygen crossover on the anode of a Li-O₂ battery using an ether-based solvent: insights from experimental and computational studies, ChemSusChem 6 (2013) 51–55.
[10] R. Younesi, M. Hahlin, M. Roberts, K. Edström, The SEI layer formed on lithium metal in the presence of oxygen: a seldom considered component in the development of the Li-O₂ battery, J. Power Sources 225 (2013) 40–45.
[11] J.-L. Shui, J.S. Okasinski, P. Kenesei, H.A. Dobbs, D. Zhao, J.D. Almer, D.-J. Liu, Reversibility of anodic lithium in rechargeable lithium–oxygen batteries, Nat. Commun. 4 (2013) 2255–2261.
[12] H.-J. Shin, W.-J. Kwak, D. Aurbach, Y.-K. Sun, Large-scale Li-O₂ pouch type cells for practical evaluation and applications, Adv. Funct. Mater. 27 (2017) 1605500.
[13] I.C. Jang, Y. Hidaka, T. Ishihara, Li metal utilization in lithium air rechargeable batteries, J. Power Sources 244 (2013) 606–609.
[14] T.T. Zuo, X.W. Wu, C.P. Yang, Y.X. Yin, H. Ye, N.W. Li, Y.G. Guo, Graphitized carbon fibers as multifunctional 3D current collectors for high areal capacity Li anodes, Adv. Mater. (2017) 1700389.
[15] Q. Yun, Y.B. He, W. Lv, Y. Zhao, B. Li, F. Kang, Q.H. Yang, Chemical dealloying derived 3D porous current collector for Li metal anodes, Adv. Mater. 28 (2016) 6932–6939.
[16] C.P. Yang, Y.X. Yin, S.F. Zhang, N.W. Li, Y.G. Guo, Accommodating lithium into 3D current collectors with a submicron skeleton towards long-life lithium metal anodes, Nat. Commun. 6 (2015) 8058–8066.
[17] A.O. Raji, R. Villegas Salvatierra, N.D. Kim, X. Fan, Y. Li, G.A.L. Silva, J. Sha, J.M. Tour, Lithium batteries with nearly maximum metal storage, ACS Nano 11 (2017) 6362–6369.
[18] B.G. Kim, J.-S. Kim, J. Min, Y.-H. Lee, J.H. Choi, M.C. Jang, S.A. Freunberger, J.W. Choi, A moisture- and oxygen-impermeable separator for aprotic Li-O₂ batteries, Adv. Funct. Mater. 26 (2016) 1747–1756.
[19] D.J. Lee, H. Lee, Y.J. Kim, J.K. Park, H.T. Kim, Sustainable redox mediation for lithium-oxygen batteries by a composite protective layer on the lithium-metal anode, Adv. Mater. 28 (2016) 857–863.
[20] P.S. Gilles Lancel, Gwenaëlle Toussaint, Manuel Maréchal, Natacha Krins, Damien Bregiroux, Christel Laberty-Robert, Hybrid Li Ion conducting membrane as protection for the Li anode in an aqueous Li–Air battery: coupling sol–gel chemistry and electrospinning, Langmiur 33 (2017) 9288–9297.
[21] Q.C. Liu, J.J. Xu, S. Yuan, Z.W. Chang, D. Xu, Y.B. Yin, L. Li, H.X. Zhong, Y.S. Jiang, J.M. Yan, X.B. Zhang, Artificial protection film on lithium metal anode toward long-cycle-life lithium–oxygen batteries, Adv. Mater. 27 (2015) 5241–5247.
[22] M. Asadi, B. Sayahpour, P. Abbasi, A.T. Ngo, K. Karis, J.R. Jokisaari, C. Liu, B. Narayanan, M. Gerard, P. Yasaei, X. Hu, A. Mukherjee, K.C. Lau, R.S. Assary, F. Khalili-Araghi, R.F. Klie, L.A. Curtiss, A. Salehi-Khojin, A lithium-oxygen battery with a long cycle life in an air-like atmosphere, Nature 555 (2018) 502–506.
[23] C.V. Amanchukwu, J.R. Harding, Y. Shao-Horn, P.T. Hammond, Understanding the chemical stability of polymers for lithium–air batteries, Chem. Mater. 27 (2015) 550–561.
[24] G.A. Umeda, E. Menke, M. Richard, K.L. Stamm, F. Wudl, B. Dunn, Protection of lithium metal surfaces using tetraethoxysilane, J. Mater. Chem. 21 (2011) 1593–1599.
[25] F. Liu, Q. Xiao, H.B. Wu, L. Shen, D. Xu, M. Cai, Y. Lu, Fabrication of hybrid silicate coatings by a simple vapor deposition method for lithium metal anodes, Adv. Energy Mater. 8 (2018) 1701744.
[26] J.-J. Xu, Q.-C. Liu, Y. Yu, J. Wang, J.-M. Yan, X.-B. Zhang, In situ construction of stable tissue-directed/reinforced bifunctional separator/protection film on lithium anode for lithium-oxygen batteries, Adv. Mater. (2017) 1606552.
[27] F. Li, R. Ohnishi, Y. Yamada, J. Kubota, K. Domen, A. Yamada, H. Zhou, Carbon supported TiN nanoparticles: an efficient bifunctional catalyst for non-aqueous Li-O₂ batteries, Chem. Commun. 49 (2013) 1175–1177.
[28] C.O. Laoire, S. Mukerjee, K.M. Abraham, E.J. Plichta, M.A. Hendrickson, Influence of nonaqueous solvents on the electrochemistry of oxygen in the rechargeable lithium–air battery, J. Phys. Chem. C 114 (2010) 9178–9186.
[29] E. Yoo, H. Zhou, Enhanced cycle stability of rechargeable Li-O₂ batteries by the synergy effect of a LiF protective layer on the Li and DMTFA additive, ACS Appl. Mater. Interfaces 9 (2017) 21307–21313.
[30] F. Huang, G. Ma, Z. Wen, J. Jin, S. Xu, J. Zhang, Enhancing metallic lithium battery performance by tuning the electrolyte solution structure, J. Mater. Chem. A 6 (2018) 1612–1620.
[31] B.M. Gallant, D.G. Kwabi, R.R. Mitchell, J. Zhou, C.V. Thompson, Y. Shao-Horn, Influence of Li₂O₂ morphology on oxygen reduction and evolution kinetics in Li–O₂ batteries, Energy Environ. Sci. 6 (2013) 2518–2528.
[32] Y.-C. Lu, B.M. Gallant, D.G. Kwabi, J.R. Harding, R.R. Mitchell, M.S. Whittingham, Y. Shao-Horn, Lithium–oxygen batteries: bridging mechanistic understanding and battery performance, Energy Environ. Sci. 6 (2013) 750–768.
[33] R.R. Mitchell, B.M. Gallant, Y. Shao-Horn, C.V. Thompson, Mechanisms of morphological evolution of Li₂O₂ particles during electrochemical growth, J. Phys. Chem. Lett. 4 (2013) 1060–1064.
[34] S.-S. Chi, X.-G. Qi, Y.-S. Hu, L.-Z. Fan, 3D flexible carbon felt host for highly stable sodium metal anodes, Adv. Energy Mater. 8 (2018) 1702764.
[35] V.S. Bryantsev, V. Giordani, W. Walker, M. Blanco, S. Zecevic, K. Sasaki, J. Uddin, D. Addison, G.V. Chase, Predicting solvent stability in aprotic electrolyte Li-air batteries: nucleophilic substitution by the superoxide anion radical (O₂⁻), J. Phys. Chem. A 115 (2011) 12399–12409.
[36] K.U. Schwenke, S. Meini, X. Wu, H.A. Gasteiger, M. Piana, Stability of superoxide radicals in glyme solvents for non-aqueous Li-O₂ battery electrolytes, Phys. Chem. Chem. Phys. 15 (2013) 11830–11839.
[37] K. Takechi, S. Higashi, F. Mizuno, H. Nishikoori, H. Iba, T. Shiga, Stability of solvents against superoxide radical species for the electrolyte of lithium-air battery, ECS Electrochem. Lett. 1 (2012) A27–A29.
[38] S.A. Freunberger, Y. Chen, N.E. Drewett, L.J. Hardwick, F. Barde, P.G. Bruce, The lithium-oxygen battery with ether-based electrolytes, Angew. Chem. Int. Ed. 50 (2011) 8609–8613.